Cite this: *Soft Matter*, 2011, **7**, 4357

www.rsc.org/softmatter

**PAPER**

# Structure and support induced structure disruption of soft nanoparticles obtained from hydroxylated fatty acids

**J. A. Heredia-Guerrero,[a] M. A. San-Miguel,[b] M. Luna,[c] E. Domínguez,[d] A. Heredia[e] and J. J. Benítez*[a]**

***Received 25th December 2010, Accepted 15th February 2011***
**DOI: 10.1039/c0sm01545h**



Soft and spherical nanoparticles, named as *cutinsomes*, have been prepared from concentrated 9(10),16-dihydroxypalmitic acid (diHPA) in aqueous solution. After isolation, cutinsomes have been chemically and structurally characterized by ATR-FTIR, TEM and dynamic atomic force microscopy (dynamic AFM). The nanoparticle can be described as a lipidic, liquid-like and mostly esterified core surrounded by a polar shell of carboxylate/carboxylic acid molecules. Molecular dynamic (MD) simulations have been used to support this model. The structural stability of soft cutinsomes has been tested by deposition on both non-polar (HOPG) and polar (mica) flat substrates. It has been found that the magnitude of the interaction between the polar shell of cutinsomes and the support determines their structure conservation or its spreading or rupture and spill out of the liquid-like content. The structural consistence of these nanoparticles as a function of the polarity of substrate is of interest in elucidating the formation mechanism of cutin, the most abundant biopolyester in nature and a very interesting biomaterial to be mimetized.

## 1. Introduction

Long chain polyhydroxy fatty acids are molecules of particular interest because they are the constituents of plant barrier polymers such as cutin and suberin. These biopolymers are extremely abundant in nature and play a very important role in protecting higher plants against physical, chemical and biological impacts as well as in regulating water loss.[1] Despite such ubiquitous presence in the biosphere, their chemical composition is rather uniform. For instance, depolymerization products of biopolyester cutin are almost exclusively composed of derivatives of the $C_{16}$ and $C_{18}$ carboxylic acids.[2,3] Among these derivatives, the 9(10),16-dihydroxypalmitic acid (diHPA) is the most abundant monomer and it is considered as the building unit of cutin, the lipid polyester that constitutes the major part of plant cuticle.

The specific interactions between long chain polyhydroxy fatty acid molecules have been studied in detail by preparing self-assembled layers from solution on a flat support like mica.[4–7] Results obtained clearly indicate that hydroxyl groups rule intermolecular interactions. Thus, hydroxyl groups in mid-chain positions reinforce the lateral interaction between packed molecules but a hydroxyl in terminal position is necessary to trigger the multilayer growth. Particularly, and if compared with related molecules, diHPA monomers lead to a very effective 2D growth covering the mica support as well as the simultaneous development of multilayers. Besides, spontaneous self-esterification within the layers has been detected.[6] These findings have brought the attention to the self-assembly route as a plausible mechanism for the biosynthesis of cutin at the wall of epidermal cells in plants.

Such basic information about self-assembly of polyhydroxy fatty acids has been obtained using solutions containing chloroform or light alcohols as solvents. However, any hypothesis about self-assembly *in vivo* has to involve an aqueous medium. In weak acid aqueous medium, polyhydroxy fatty acids give rise to nanometre sized lipid spherical particles.[8] It has also been demonstrated that these nanoparticles (cutinsomes) are involved in the genesis of cutin of young fruits during development. [9] The soft structure of cutinsomes requests special care and the employment of high sensitivity and non-destructive analysis techniques. Among them, dynamic atomic force microscopy (dynamic AFM) provides a very high topographic resolution with negligible sample perturbation. This AFM mode is based on the change in oscillation amplitude of the cantilever due to the effect of attractive non-linear van der Waals forces.[10–12] The main difference with respect to intermittent contact (tapping) is that parameters can be adjusted for non-contact operation: the tip does not usually reach the adhesive or repulsive contact with the surface. Therefore, while keeping the resolution power of tapping mode, the possibility of sample damage is further reduced. This

[a]*Instituto de Ciencia de Materiales de Sevilla, Centro Mixto CSIC-Universidad de Sevilla, Avda, Americo Vespuccio 49, 41092 Seville, Spain. E-mail: benitez@icmse.csic.es*
[b]*Departamento de Química-Física, Facultad de Química, Universidad de Sevilla, 41012 Seville, Spain*
[c]*Instituto de Microelectrónica de Madrid (IMM-CSIC), 28760 Tres Cantos, Madrid, Spain*
[d]*Estación Experimental "La Mayora" (CSIC), Algarrobo-Costa, 29750 Málaga, Spain*
[e]*Departamento de Biología Molecular y Bioquímica, Universidad de Málaga, 29071 Málaga, Spain*

technique has been extensively used to image the topography of delicate samples such as physisorbed supramolecular three dimensional architectures[13] or even liquid droplets[10] and films.[14] In this article, structural data obtained from TEM and dynamic AFM are also supported with molecular dynamic (MD) simulations.

From a biological point of view, the possibility of biopolyester cutin formation in nature through cutinsomes packing, aggregation and fusion at the epidermis of plant cell walls is very plausible. This hypothesis drives the analysis to the nanoparticle self-assembly rather than to the discrete molecular packing. In this sense, the physical and chemical properties of the support are very important factors in controlling the mechanism of cutinsomes accretion. For this reason, this study comprises two model supports such as HOPG (non-polar, hydrophobic) and mica (polar, hydrophilic). The aim is to obtain general conclusions that can later be transferred to the actual and particular conditions acting at the vegetal epidermal cell walls.

## 2. Experimental section

### 2.1. Lipid nanoparticle preparation

9(10),16-Dihydroxypalmitic acid (diHPA) is not a commercial product and has been obtained by depolymerization in aqueous solution of NaOH 1 M of plant cutin from enzymatically isolated cuticles of tomato fruits following a procedure already reported.[15] Cutinsomes were prepared starting with filtered 10 mM diHPA aqueous alkaline solutions at pH 12.5 and reducing the pH to 6.8 with small amounts of HCl.[16] The solution becomes then opalescent and nanoparticles were obtained after centrifugation at 19 000*g*. The product is washed several times with distilled water and filtered. Dispersions are prepared using 1.5 mg of cutinsomes in 1.5 mL of distilled water and sonicated for 1 h.

### 2.2. ATR-FTIR

*ATR-FTIR* spectra of samples were obtained from pellets of purified cutinsomes using an ATR accessory (MIRacle ATR, PIKE Technologies, USA) coupled to FTIR spectrometer (FT/IR-4100, JASCO, Spain). All spectra were recorded in the 4000 to 600 $cm^{-1}$ range at 4 $cm^{-1}$ resolution and 250 scans were accumulated.

### 2.3. TEM

For TEM analysis, a small drop of dispersion of cutinsomes in water was deposited on a copper grid. Nanoparticles were stained with an aqueous uranyl acetate solution 1% (w/v). The grids were analyzed at 100 kV with a Philips CM 100 electron microscope.

### 2.4. MD simulations

Molecular dynamic simulations were performed with DL_POLY[17] using the NVT ensemble with a Nosé–Hoover thermostat[18] at 300 K. The initial velocities were set up from a Boltzmann distribution. The equations of motion were integrated by using the velocity-Verlet algorithm with a time step of 1 fs. Simulations were extended up to 4 ns. The interatomic potential parameters were taken from literature and have been used already in previous studies.[6,7] A united atom model was employed for $–CH_3$ and $–CH_2–$ groups and all the other atoms in hydroxyl and carboxylic groups were represented explicitly. A cutoff radius of 15 Å was used for the Lennard-Jones (6–12) potential terms. The electrostatic interactions were treated using the method of Hautman and Klein which is an adaptation of the Ewald method for systems which are periodic in two dimensions only.[19] Molecules were deposited on a substrate represented as a flat surface and the interaction between each particle and the surface was computed according to:

$$V(r) = \frac{C_{12}}{(z - z_0)^{12}} - \frac{C_3}{(z - z_0)^3}$$

where $C_n\alpha(\sigma\varepsilon^n)^{1/2}$, $z$ is the distance to the surface and $z_0$ is a limit approach distance for each center. $\varepsilon$ and $\sigma$ are Lennard-Jones potential parameters and they were calculated using the Lorentz–Berthelot combining rules. $C_n$ parameters for $CH_2$ and O particles were taken and adapted from the literature.[20]

### 2.5. Cutinsome deposition for dynamic AFM

Two preparation methods: (i) drop vaporization and (ii) spin coating, have been used. In both cases, a droplet (25 μL) of the aqueous dispersion of cutinsomes was deposited on the freshly cleaved substrate (HOPG, ZYB quality, or mica, muscovite). In drop vaporization method, water was allowed being evaporated slowly by keeping the sample at 6 °C for 24 h. In the spin coating method, the samples were spun at 40 rps for 30 s.

### 2.6. Dynamic AFM operation

The AFM is a Cervantes model from Nanotec Electrónica (Spain) operated at room conditions (20–25 °C and 35–40% RH). Images were obtained and processed using the WSxM software.[21] Nanosensors $Si_3N_4$ rectangular cantilevers with nominal force constant of 2.8 N $m^{-1}$ and resonance frequency around 80 kHz were used.

Parameters such as the cantilever driving oscillation amplitude, force constant, resonance frequency and oscillation amplitude set point have to be carefully selected and optimized for the operation out of contact.[22] Out of contact conditions can be obtained at typically 1–5 nm from the surface.[23–25]

## 3. Results and discussion

### 3.1. Infrared spectroscopy characterization of cutinsomes

Fig. 1 shows the infrared spectra of cutinsomes obtained from diHPA. A broad medium intensity band at 3327 $cm^{-1}$ is indicative of the stretching vibration of hydrogen bonded hydroxyl groups. The frequency value is in the range of intermolecular hydrogen bonds that give rise to polymeric associations[26,27] and therefore suggests a strong crosslinking between the alkyl chains. A residual phase with a more relaxed hydrogen bonding is revealed by the shoulder at 3460 $cm^{-1}$.

Strong asymmetrical and symmetrical stretching vibrations of methylene ($–CH_2–$) groups are located at 2924 and 2851 $cm^{-1}$, respectively. The position of these bands is a good parameter to



 

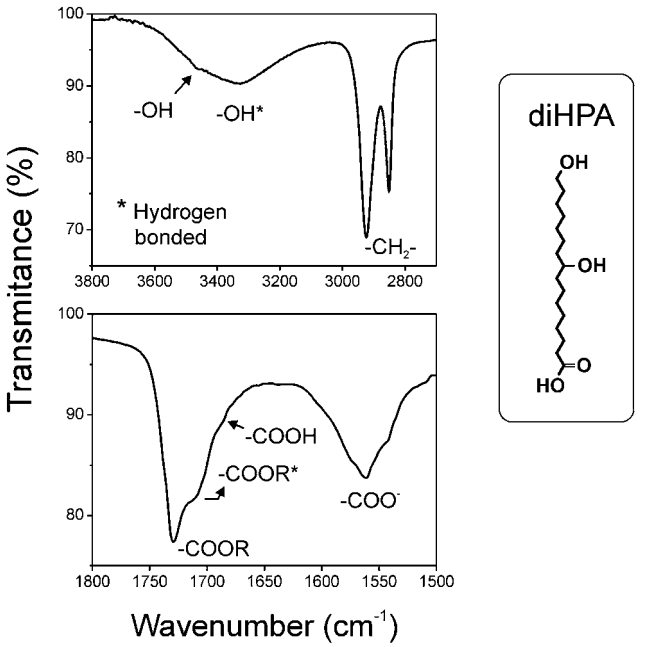


**Fig. 1** ATR-FTIR spectra of cutinsomes obtained from 9(10),16-dihydroxypalmitic acid (diHPA). Both the presence of an ester and a –COOH/–COO⁻ phase are detected. The structure of diHPA molecule is schematized on the right side.

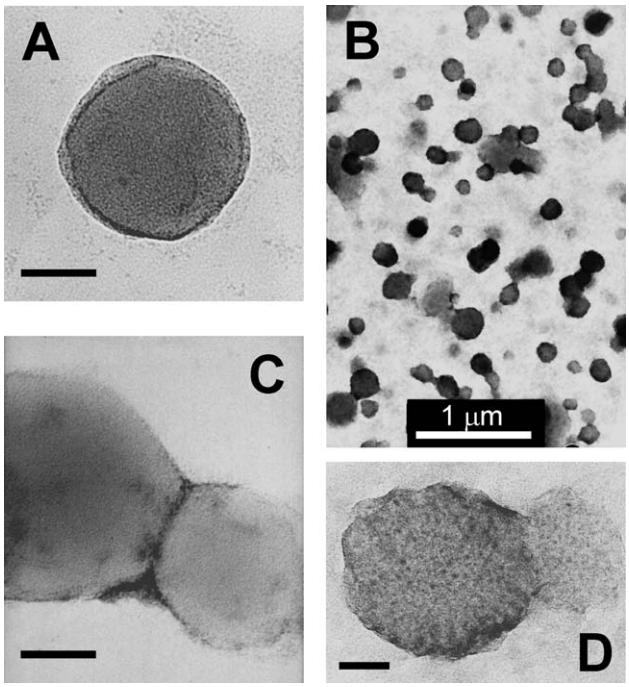


**Fig. 2** TEM micrographs of purified cutinsomes showing their spherical shape. Both isolated (A and B), aggregated (B and C) and broken (B and D) units can be detected. Black scale bar is 50 nm.

evaluate the rigidity of the alkyl chain framework.[28] The band at 2851 $cm^{-1}$ represents an intermediate state between a fluid (2854 $cm^{-1}$) and a rigid (2849 $cm^{-1}$) phase.[29,30]

The spectral region between 1800 and 1500 $cm^{-1}$ corresponds to the stretching vibrations of (C=O) in ester, carboxylic and carboxylate groups and it has been characterized in great detail.[8,31] In this zone, the main band appears at 1730 $cm^{-1}$ with two shoulders at 1712 and 1687 $cm^{-1}$. The 1730 $cm^{-1}$ peak and the 1712 $cm^{-1}$ shoulder is assigned to free and hydrogen bonded esters, respectively. The C=O vibration of free carboxylic acid is represented by the shoulder at 1687 $cm^{-1}$. The band contour confirms a high degree of esterification and the minor presence of free carboxylic acid and hydrogen-bonded C=O groups. Another evidence of esterification is the 1166 $cm^{-1}$ asymmetric C–O–C stretching (not shown in the figure).

On the other hand, the presence of carboxylate ($–COO^-$) groups is significant, as indicated by the 1561 $cm^{-1}$ and the 1412 $cm^{-1}$ (not shown in the figure) peaks, respectively assigned to the corresponding asymmetrical and symmetrical C=O stretching.

### 3.2. Transmission electron microscopy (TEM)

TEM images of cutinsomes typically show aggregated or fused spherical structures, but also isolated nanoparticles can be detected (Fig. 2). Nanoparticle diameter is about 50–200 nm. The TEM image displayed in Fig. 2D is of particular interest because it shows a low contrast structure associated to a bigger and denser nanoparticle. Wrinkles in the darker body, as well as the lack of a border between the two phases (compare Fig. 2C and D), suggest the open up and spreading of the liquid-like content of the original cutinsome. This observation is in good agreement with ATR-FTIR results which indicated a crosslinked non-rigid esterified phase with hydroxyl group associated in a hydrogen bonded network. The carboxylate/carboxylic ($–COO^-$/–COOH) phase would define the nanoparticle shell separating the lipidic content from the aqueous preparation medium.

### 3.3. Molecular dynamic simulations

To better understand and describe the structure of cutinsomes, we have carried out molecular dynamic simulations assuming a model in which the nanoparticle is divided in two parts: shell and core.

The shell is the border between the aqueous medium and the lipidic content. This part is very likely characterized by the exposure of the more hydrophilic –COOH/$–COO^-$ groups towards the aqueous medium. The lipidic core does not have such requirement of exposing the carboxylic group and, therefore, the lack of a preferential molecular orientation is presumed. Consequently, in the simulations, two different starting configurations of 9,16-dihydroxypalmitic acid molecules are adopted. The first one (Fig. 3A), intends to mimic the internal region (core) of the cutinsome. In this case 100 diHPA molecules in all-*trans* configuration were arranged in parallel at constant intermolecular distance of 5.2 Å in a triangular lattice. The molecules were oriented with the –COOH group facing the surface (down) or in the opposite direction (up) alternatively, resulting in 50% of the molecules in each orientation. These molecules constitute a first layer separated from the surface at 3 Å. A second layer identical to the first one was placed at 3 Å from the upper atoms in the first layer. The modelization in two layers is to account for the three dimensional character of the core and the alternative up and down distribution for the lack of a superimposed molecular orientation within the lipidic phase. diHPA molecules are then

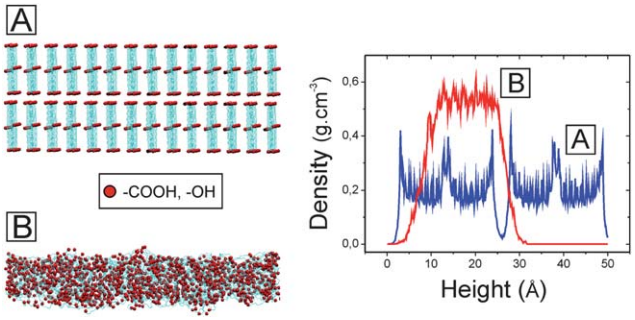


**Fig. 3** (A) Starting up and down diHPA molecular arrangement used for the MD simulations of the cutinsome core. (B) Final state after 2 ns simulation. Red circles represent the oxygen atoms in carboxylic and hydroxyl groups. The alternated ordered configuration readily evolves to a disordered, cross-linked and denser state, as observed from the corresponding density profiles (A to B).

able to interact with each other *via* intra- or inter-layer with different orientations.

On the other side, the outer shell (Fig. 5A) only comprises a single monolayer of 100 diHPA molecules in parallel and with the –COOH groups facing the surface (down orientation) at constant intermolecular distance of 5.2 Å in a triangular lattice. This uniformly oriented distribution is consistent with the preferential exposing of polar hydrophilic groups towards the aqueous medium. Modelization in a single layer arises from the interface role of the shell separating the core from the outside. Periodic conditions were imposed along the *X* and *Y* directions in both systems.

Simulations in the core model indicate that the initial ordered state quickly evolves towards a disordered and denser configuration (Fig. 3B). Disordering is evident from the density profiles as the sharp peaks due to the ordered positions of the –COOH and –OH groups vanish into a plateau. Phase densification is also deduced from the layer height which decreases from ~50 Å to ~30 Å. As it has been demonstrated previously[6,7] these systems are susceptible to self-esterification, particularly when there is an adequate molecular orientation for the nucleophilic attack and the formation of water. In order to gain insight into the esterification process, the radial distribution functions (RDFs) have been computed. The most relevant profiles correspond to $\delta_1$ (the distance between the carbon atom of carbonyl in –COOH groups and the oxygen atom in hydroxyl groups) and $\delta_2$ (the distance between the hydrogen atom in hydroxyl groups and the oxygen in the hydroxyl group within –COOH groups) (scheme in Fig. 4). For $\delta_1$, initially, there are two wide bands centred about 5.0 and 10.5 Å corresponding to distances between carbonyl and primary and secondary hydroxyl groups, respectively. After 2 ns simulation, there is a distinct peak at 3.7 Å related to the approaching distance in a nucleophilic attack to form an ester. For $\delta_2$ distance, there is a fairly flat profile initially, but exhibiting distinct peaks as the simulation proceeds. Particularly, the peak at 1.9 Å indicates an important short distance which is attributed to the formation of a water molecule. These classical simulations are not able to reproduce bond breaking and/or bond formation processes, however, these results constitute a strong evidence of the molecular rearrangement towards the esterification reaction, *i.e.* the initial stage of a cross-linking process.

The conclusion is that when intermolecular interactions predominate, as presumed in the bulk of cutinsomes, diHPA molecules have a strong tendency to cross-link and self-esterify. Two bonding networks are then defined, a primary one created by ester bonds and a secondary one made of hydrogen bonded hydroxyl groups. These findings are consistent with infrared spectroscopy data.

In the case of cutinsome shell, simulations show that the starting structure is mostly preserved (Fig. 5). Some molecular rearrangement takes place in order to favour the formation of the hydrogen bonding network between primary or secondary hydroxyl groups and some ester bonds between secondary hydroxyls and carboxylic groups. However, the interaction with

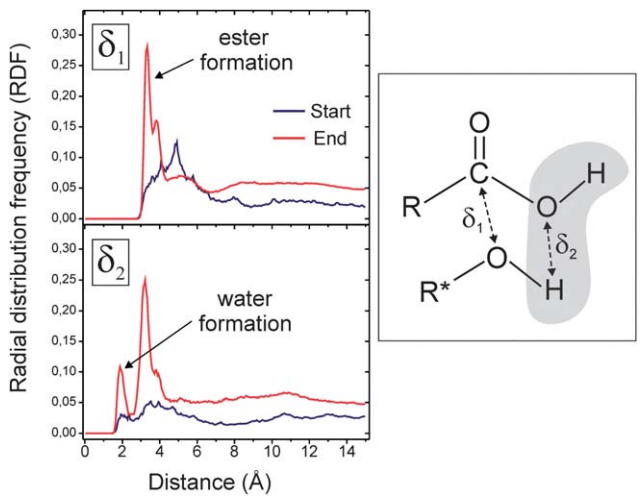


**Fig. 4** Radial distribution functions corresponding to the nucleophilic attack ($\delta_1$) and the formation of the water molecule ($\delta_2$) as requested by the occurrence of the self-esterification reaction between diHPA molecules at the cutinsome core (scheme). After simulation convergence, characteristic $\delta_1$ (3.7 Å) and $\delta_2$ (1.9 Å) are defined indicating that the self-esterification reaction is feasible.

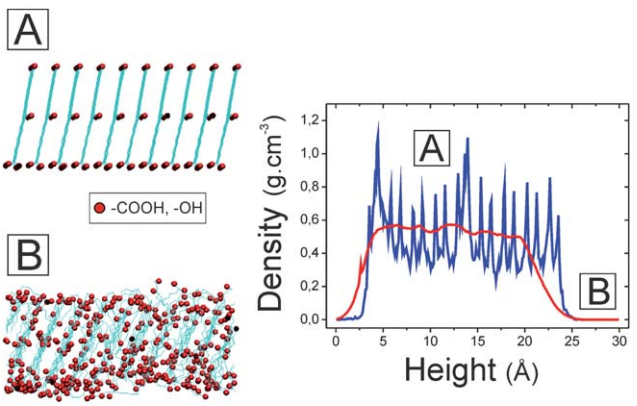


**Fig. 5** (A) Starting and (B) final molecular arrangements from MD simulations corresponding to the modelling of the outer shell of cutinsomes. Red circles represent the oxygen atoms in carboxylic and hydroxyl groups. No significant structure modification is observed indicating that an ordered –COOH/–$COO^-$ monolayer cap surrounding the cutinsome is a stable configuration.

 

the substrate is still strong enough to keep the latter ones facing the surface and display a rather vertical orientation for an extended simulation time. This fact can be observed quantitatively from the tilt angle between the diHPA long axis and the surface normal, which has been computed from the moment of inertia matrix. The corresponding angular frequency distributions show an average tilt of 20–25°. Identical results are obtained when simulations are extended to a bilayer of diHPA.[6] This is interpreted as when an external potential is forcing diHPA molecules to orientate in the same direction, as is presumed for the cutinsome shell towards the aqueous medium, intermolecular interactions are not enough to modify this configuration.

### 3.4. Dynamic atomic force microscopy

A very important issue to be addressed in this article is whether the soft nanoparticle structure is affected by its interaction with a support. For this purpose, two reference substrates such as mica (polar) and HOPG (non-polar) and an extremely low perturbing analysis technique such as dynamic atomic force microscopy have been used.

**3.4.1. Cutinsomes on mica.** Fig. 6 shows the type of structures that are found when a drop of the cutinsomes dispersion is slowly vaporized on mica. Fig. 6A corresponds to the most representative situation: a homogeneous distribution of relatively small flat islands, 200–300 nm in diameter and about 4.5 nm high. Associated to the flat island, higher (10–20 nm) features (dots) are observed. As previously indicated, cutinsomes in aqueous dispersion are envisaged as soft nanoparticles with an inner liquid-like framework made of crosslinked and mostly esterified monomers surrounded by a polar shell (mainly carboxylic and carboxylate groups). It is reasonable then to expect a strong interaction between mica and the nanoparticle shell causing its spread up and/or its open up and the release of its content. The reference for this spreading/rupture of cutinsomes is the study of adsorption and self-assembly of discrete diHPA molecules from solution on mica. diHPA molecules do self-assemble forming well defined multilayered deposits as a function of solution concentration.[6] According to these previous data, the higher features (dots) in Fig. 6A correspond to the more rigid crosslinked and esterified skeleton of the cutinsome, while the flat islands are the result of the self-assembly of the more relaxed phase, the residual free monomers and the carboxylate/carboxylic shell on the support. The lower height of flat islands in Fig. 6A (4.5 nm high) compared to the diHPA bilayer (5 nm high) is an indication of some degree of cross-linking within the self-assembled phase, as suggested by the MD simulations (Fig. 3).

A simple calculation to determine the diameter of an island 4.5 nm high resulting from full spreading of a sphere content with the average size of a cutinsome (50 nm in diameter) yields about 135 nm, which is within the island size range observed in Fig. 6A. Larger islands are the result of the already described tendency of cutinsomes to aggregate and fuse into bigger particles. Also, the size of the higher features assigned to the more rigid cutinsome skeleton (10–20 nm high, 20–50 nm in diameter) is compatible with the inner volume of a cutinsome.

Occasionally, multilayered deposits displaying discrete steps 2.5 nm high are observed (Fig. 6B). As the step height observed corresponds to the diHPA molecular length (2.5 nm), this is considered to be the result of non-crosslinked carboxylic acid and carboxylate molecular self-assembly from cutinsomes with a low esterification degree.

When prepared by spin coating very similar results are obtained. The only difference is the formation of additional rounded islands 2.3 nm high with an average diameter of about 300 nm. Again, the volume associated to these islands is in good concordance with the volume of a sphere with a diameter of 60–70 nm. The formation of such monolayer islands can be understood by the action of centrifugal forces while spinning in a better spreading of both the cutinsomes and the particle content.

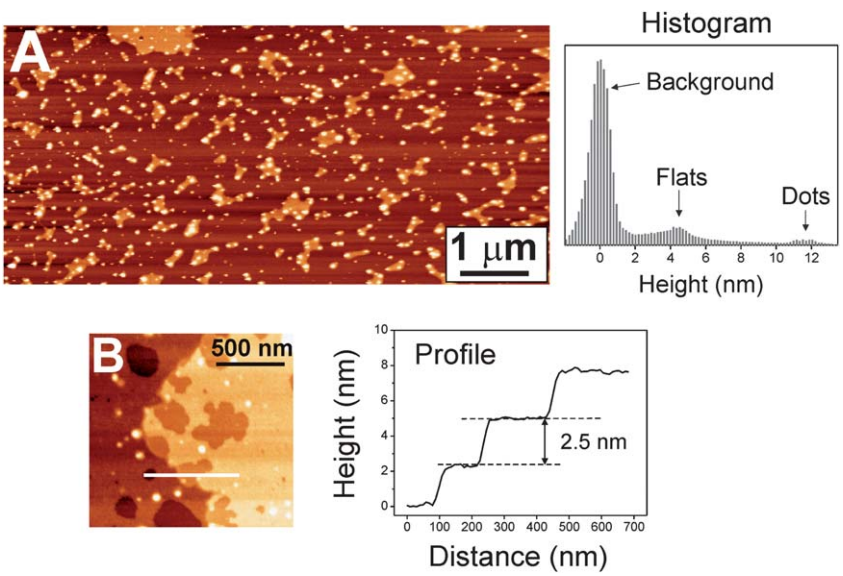


**Fig. 6** Dynamic AFM images of purified cutinsomes deposited on mica by drop vaporization. Topographic data suggest the cutinsome spreading or break up and the self-assembly of the liquid-like content into layered islands. See text for A and B cases.

**3.4.2. Cutinsomes on graphite.** On graphite, the wetting of the droplet is low and the structure of the deposit is strongly affected by concentration gradients along solvent evaporation. Fig. 7 shows the topographic images obtained after cutinsomes drop vaporization on HOPG. The images are ordered from the edges to the centre of the deposited droplet (A to C). A very clear densification of the deposit upon slow retraction of the solvent towards the centre of the droplet is observed.

The lower density region (Fig. 7A) displays a thin and smooth globular layer covering the substrate (still graphite terraces are visible). The background RMS roughness is quite low (0.4–0.5 nm).

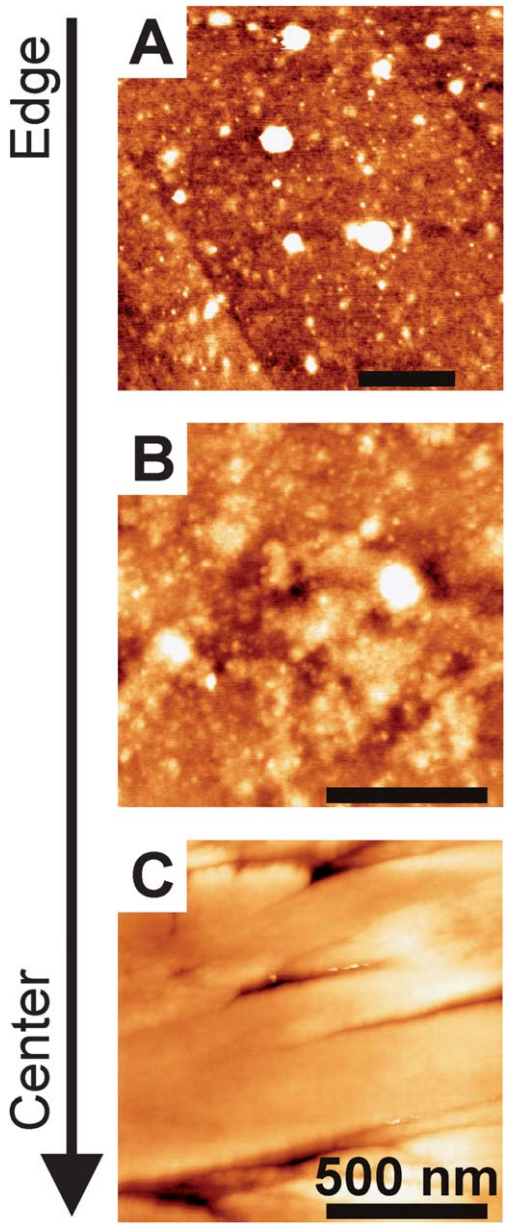


**Fig. 7** Dynamic AFM images of purified cutinsomes deposited on HOPG by drop vaporization. The globular structure gets denser on going from the edge towards the centre of the deposited drop. Topographic data suggest a strong cutinsome aggregation rather than nanoparticle break up. See text for A to C cases.

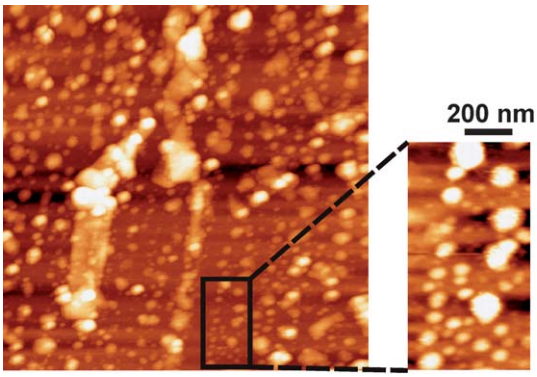


**Fig. 8** Dynamic AFM images of purified cutinsomes deposited on HOPG by spin coating. Isolated rounded features are detected indicating that no nanoparticle spreading or break up occurs on non-polar substrates.

Roughness increases upon densification of the deposit (Fig. 7B) until a thick continuous layer is formed (Fig. 7C). Topographic data suggest the progressive aggregation and fusion of cutinsomes to form this continuous layer. The low polarity of HOPG substrate seems to favour the particle accretion and prevents content release as observed on mica.

To study the structure of single cutinsomes and its interaction with HOPG, the tendency of aggregation has to be hindered. This is achieved by using the spin-coating preparation method. Dynamic AFM images of spin-coated samples (Fig. 8) show isolated rounded features with a diameter ranging from 50 to 150 nm, which is in good agreement with the size of isolated cutinsomes observed by TEM. Still some aggregation takes place giving rise to bigger particles. Also, in some areas small crystallites can be observed, probably caused by the local fast drying of the thin liquid layer created by spin-coating.

## 4. Conclusions

Nanometer sized particles named as cutinsomes have been prepared and isolated from concentrated aqueous solutions of 9(10),16-dihydroxypalmitic acid (diHPA). Chemically cutinsomes are characterized as a mostly esterified phase resulting from the reaction between carboxylic acid (–COOH) and hydroxyl (–OH) groups. ATR-FTIR also detects a significant presence of free carboxylate ($–COO^-$) and a hydrogen bonded network involving non-reacted hydroxyls. TEM analysis of these nanoparticles has revealed it as a sphere-like structure with diameters ranging from 50–200 nm. Detailed analysis of the frequency of methylene group stretching vibration indicates a non-rigid alkyl chain structure. Based on this, the cutinsome nanoparticle is defined as a mostly esterified liquid-like core containing some free monomeric units and surrounded by a –COOH/$–COO^-$ shell separating the lipidic content from the aqueous environment. Molecular dynamic simulation results are consistent with this model. Dynamic AFM images of cutinsomes have revealed that their interaction with the support can control their spherical structure disruption. Polar substrates such as mica induce the particle rupture or spreading and the self-assembly of the liquid-like content driven by the strong interaction with the

 

–COOH/–$COO^-$ shell. However, non-polar substrates such as HOPG preserve the nanoparticle structure.

The structure and capacity of cutinsomes to aggregate and undergo self-esterification is of particular interest because they have been proposed as the building units of cutin, the most abundant polyester in nature and a very interesting material to be mimetized as a bioplastic.[30] The capability of the support in preserving the integrity of such nanoparticles is an important factor in elucidating the transport mechanism across the plant cell walls in the biosynthetic pathway of cutin.

## Acknowledgements

This research work has been funded by the Consejería de Innovación Ciencia y Empresa (Junta de Andalucía) through the TEP-02550 project and the EPSRC and BBSRC (*via* the Bionanotechnology IRC).

## References

1 K. Roberts, *Handbook of Plant Science*, Wiley, Chichester, 2007, vol. 1.
2 A. Heredia, *Biochim. Biophys. Acta, Gen. Subj.*, 2003, **1620**, 1.
3 M. Riederer and C. Muller, *The Biology of Plant Cuticle*, Blackwell, London, 2005.
4 J. J. Benítez, J. A. Heredia-Guerrero and A. Heredia, *J. Phys. Chem. C*, 2007, **111**, 9465.
5 J. J. Benítez, J. A. Heredia-Guerrero, F. Serrano and A. Heredia, *J. Phys. Chem. C*, 2008, **112**, 16968.
6 J. A. Heredia-Guerrero, M. A. San-Miguel, M. S. P. Sansom, A. Heredia and J. J. Benítez, *Langmuir*, 2009, **25**, 6869.
7 J. A. Heredia-Guerrero, M. A. San-Miguel, M. S. P. Sansom, A. Heredia and J. J. Benítez, *Phys. Chem. Chem. Phys.*, 2010, **12**, 10423.
8 (*a*) J. A. Heredia-Guerrero, J. J. Benítez and A. Heredia, *BioEssays*, 2008, **30**, 273; (*b*) A. Heredia, J. A. Heredia-Guerrero, E. Domínguez and J. J. Benítez, *Biointerphases*, 2008, **4**, 1.
9 E. Domínguez, J. A. Heredia-Guerrero, J. J. Benítez and A. Heredia, *Mol. BioSyst.*, 2010, **6**, 948.
10 B. Anczykowski, D. Krüger, K. L. Babcock and H. Fuchs, *Ultramicroscopy*, 1996, **66**, 251.
11 A. Kühle, A. H. Sørensen and J. Bohr, *J. Appl. Phys.*, 1997, **81**, 6562.
12 M. Luna, J. Colchero and A. M. Baró, *J. Phys. Chem. B*, 1999, **103**, 9576.
13 M. Fuss, M. Luna, D. Alcántara, J. M. de la Fuente, P. M. Enríquez-Navas, J. Angulo, S. Penadés and F. Briones, *J. Phys. Chem. B*, 2008, **112**, 11595.
14 A. Gil, J. Colchero, M. Luna, J. Gómez-Herrero and A. M. Baró, *Langmuir*, 2000, **16**, 5086.
15 P. Luque, S. Bruque and A. Heredia, *Arch. Biochem. Biophys.*, 1995, **317**, 417.
16 C. L. Apel, D. W. Deamer and M. N. Mautner, *Biochim. Biophys. Acta, Gen. Subj.*, 2002, **1559**, 1.
17 W. Smith, C. W. Yong and P. M. Rodger, *Mol. Simul.*, 2002, **28**, 385.
18 (*a*) S. Nose, *Mol. Phys.*, 1984, **52**, 255; (*b*) S. Nose, *J. Chem. Phys.*, 1984, **81**, 511; (*c*) available at www.ccp5.ac.uk/DL_POLY.
19 J. Hautman and M. L. Klein, *Mol. Phys.*, 1992, **75**, 379.
20 (*a*) J. Hautman and M. L. Klein, *J. Chem. Phys.*, 1989, **91**, 4994; (*b*) R. P. S. Fartaria, F. F. M. Freitas and F. M. S. S. Fernandes, *J. Electroanal. Chem.*, 2005, **574**, 321; (*c*) R. P. S. Fartaria, F. F. M. Freitas and F. M. S. S. Fernandes, *J. Braz. Chem. Soc.*, 2004, **15**, 224.
21 I. Horcas, R. Fernández, J. M. Gómez-Rodríguez, J. Colchero, J. Gómez-Herrero and A. M. Baró, *Rev. Sci. Instrum.*, 2007, **78**, 1.
22 M. Luna, J. Colchero, J. Gómez-Herrero and A. M. Baró, *Appl. Surf. Sci.*, 2000, **157**, 285.
23 M. Luna, J. Colchero and A. M. Baró, *Appl. Phys. Lett.*, 1998, **72**, 3461.
24 P. J. de Pablo, J. Colchero, M. Luna, J. Gómez-Herrero and A. M. Baró, *Phys. Rev. B: Condens. Matter*, 2000, **61**, 14179.
25 M. Köber, E. Sahagún, M. Fuss, F. Briones, M. Luna and J. J. Sáenz, *Phys. Status Solidi RRL*, 2008, **2**, 138.
26 L. J. Bellamy, *The Infrared Spectra of Complex Molecules*, Chapman and Hall, London, 1975, vol. 1.
27 L. P. Kuhn, *J. Am. Chem. Soc.*, 1952, **74**, 2492.
28 V. Velkova and M. Lafleur, *Chem. Phys. Lipids*, 2002, **117**, 63.
29 J. P. Douliez and A. Heredia, *Biomacromolecules*, 2005, **6**, 30.
30 J. A. Heredia-Guerrero, A. Heredia, R. García-Segura and J. J. Benítez, *Polymer*, 2009, **50**, 5633.
31 J. A. Heredia-Guerrero, E. Domínguez, M. Luna, J. J. Benítez and A. Heredia, *Chem. Phys. Lipids*, 2010, **163**, 329.